

Trans4Map: Revisiting Holistic Top-down Mapping from Egocentric Images to Allocentric Semantics with Vision Transformers

Chang Chen, Jiaming Zhang*, Kailun Yang, Kunyu Peng, Rainer Stiefelhagen
CV:HCI Lab, Karlsruhe Institute of Technology

Abstract

Humans have an innate ability to sense their surroundings, as they can extract the spatial representation from the egocentric perception and form an allocentric semantic map via spatial transformation and memory updating. However, endowing mobile agents with such a spatial sensing ability is still a challenge, due to two difficulties: (1) the previous convolutional models are limited by the local receptive field, thus, struggling to capture holistic long-range dependencies during observation; (2) the excessive computational budgets required for success, often lead to a separation of the mapping pipeline into stages, resulting the entire mapping process inefficient. To address these issues, we propose an end-to-end one-stage Transformer-based framework for Mapping, termed Trans4Map. Our egocentric-to-allocentric mapping process includes three steps: (1) the efficient transformer extracts the contextual features from a batch of egocentric images; (2) the proposed Bidirectional Allocentric Memory (BAM) module projects egocentric features into the allocentric memory; (3) the map decoder parses the accumulated memory and predicts the top-down semantic segmentation map. In contrast, Trans4Map achieves state-of-the-art results, reducing 67.2% parameters, yet gaining a +3.25% mIoU and a +4.09% mBF1 improvements on the Matterport3D dataset.¹

1. Introduction

Holistic scene understanding has a crucial role in both indoor and outdoor applications, *e.g.*, autonomous driving [31, 46, 48, 51], indoor exploration and navigation [18, 23, 29, 33], as well as indoor and outdoor mapping [6, 7, 12]. These tasks are ordinary for humans with excellent spatial perception ability, as they can continuously extract information from the egocentric perspective, and construct the scene semantic map in the allocentric perspective through the memory and spatial transformation.

*Corresponding author (e-mail: jiaming.zhang@kit.edu).

¹Code will be made publicly available at [Trans4Map](#).

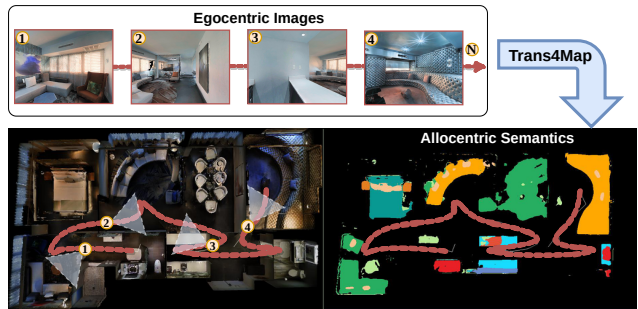


Figure 1: **The egocentric-to-allocentric semantic mapping.** Given a front-view image sequence of length N observed along a trajectory (the red dash line), Trans4Map performs the extract-project-segment pipeline, yielding an allocentric semantic segmentation map in a top-down view.

However, the semantic mapping is still difficult for an artificial intelligent mobile agent, *i.e.*, an AI assistant, particularly when exploring an unfamiliar environment. Traditional methods require huge efforts to scan the whole scene and construct maps with SLAM technology via 3D point clouds [14]. To equip a mobile agent with the surrounding sensing ability to perform the top-down semantic mapping from RGB observations, we focus on the image-based semantic mapping task, by predicting allocentric semantic segmentation from egocentric images. As the example shown in Fig. 1, given a trajectory in the scene, which is composed of a batch of first-view RGB images and the corresponding known camera pose, the mobile agent performs three steps: (1) extracting rich and compact contextual features; (2) projecting and updating the egocentric features in the intermediate allocentric memory as spatial-semantic representation of the complex spaces; (3) parsing and predicting the final top-view semantic mapping via the decoder. Compared to the SLAM-based method [14], such an image-based egocentric-to-allocentric mapping pipeline is more in line with human intuition, and is able to perform mapping in an efficient way, avoiding the need for a time-consuming reconstruction phase. For semantic mapping of egocentric images, previous works, *e.g.*, SMNet [4] have to separate the model into two stages, using a CNN-based frozen se-

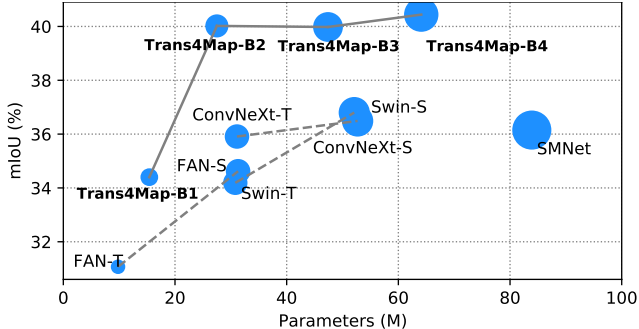


Figure 2: Semantic mapping scores (mIoU) evaluated by CNN- and Transformer-based backbones with different numbers of parameters (M). Trans4Map models achieve better results yet with fewer parameters.

semantic segmentation model to extract features in the first stage and then decoding the spatial memory to produce final semantics in the second stage, which results in a huge resource demand and time consuming.

Recently, the vision transformer architecture [42] has achieved success in different vision tasks [9, 32, 43, 44, 47, 50]. Compared to the convolutional counterparts with a narrow receptive field, the transformer-based model is able to capture long-distance contextual dependencies, forming a non-local representation, which is crucial for the holistic scene understanding. Thanks to the excellent feature modeling capability of the transformer-based model, we revisit the top-down mapping from egocentric images to allocentric semantic with a transformer-based model and put forward a novel end-to-end one-stage *Trans4Map* framework.

There are two primary benefits of Trans4Map: (1) the long-range feature modeling ability of the transformer model is advantageous to obtain a more comprehensive spatial representation during the egocentric observation process; (2) the efficient and lightweight model structure enables an end-to-end mapping process. Besides, unlike the previous method [4] using a single GRU cell on the spatial memory, we propose a novel *Bidirectional Allocentric Memory (BAM)* to produce a more meaningful representation, combining projected allocentric features from both directions. *BAM* is able to accumulate the incoming observations per each time step and avoid the occluded objects to be classified as other category, *e.g.*, chair under table.

Based on the Trans4Map framework, we delve deep into the semantic mapping task and investigate a vast number of advanced deep architectures [25, 26, 45, 53] together with learning modalities with bidirectional cross-stream fusion. To verify our proposed methods, we conduct extensive experiments and ablation studies on the Matterport3D dataset [5] and the Replica dataset [39], which contain photo-realistic scans of building-scale indoor environments using the Habitat simulation platform [37]. As shown in Fig. 2, our lightweight Trans4Map models have much fewer

parameters, yet achieve surprising semantic mapping scores and set a new state-of-the-art of a $>40\%$ mIoU on the challenging Matterport3D dataset.

To summarize, we present the following contributions:

- Rethink the top-down semantic mapping task by using a transformer-based model to parse indoor RGB observations and predict the semantic top-down map.
- Propose an end-to-end *Transformer for Mapping (Trans4Map)* framework to generate the allocentric semantic segmentation map from egocentric RGB images with known camera pose, yielding a holistic dense understanding for indoor exploration.
- Put forward a novel *Bidirectional Allocentric Memory (BAM)* which accumulates and projects the egocentric feature to the allocentric spatial tensor, via combining memories from two directions.
- Our framework outperforms state-of-the-art counterparts on both the Matterport3D dataset and the Replica dataset, while using a more lightweight model.

2. Related Work

Semantic Mapping. Recently, a number of approaches have emerged around semantic mapping. Semantic SLAM pipelines [14, 34] follow the paradigm of predicting egocentric images to top-view semantic segmentation. Such methods forward the 2D observations into a segmentation network and then use a data association strategy to project annotated labels onto the top-view map. These efforts follow the paradigm of segmentation before projection, which is particularly rigorous for depth information, *i.e.*, the global coordinates of each pixel in RGB images. Unfortunately, a slight error can lead to an offset in the projection, as well as an under-fitting of model training. Another paradigm is to convert a first-view image into the top-down view and then perform semantic segmentation based on the converted image [38]. This method loses a vast amount of visual information during the projection phase, when the model is trained to extract first-view features. In contrast, SMNet [4] trains an encoder to extract the image context features, then transform the features into a map perspective and perform semantic segmentation. However, SMNet trains the encoder and decoder separately and does not optimize the training process from the first perspective input to the generation of top-view semantics as a whole.

Lu *et al.* [27] proposed an end-to-end network encoding the front-view visual information of the driving scene utilizing a variational encoder-decoder network [20] and then decoding it into a 2D top-view Cartesian coordinate system. Pan *et al.* [30] represented a cross-view semantic segmentation network with a View Parsing Network (VPN) - an MLP that parses semantics across different views. Both methods predict a local semantic top-down map with an end-to-end network from egocentric observa-

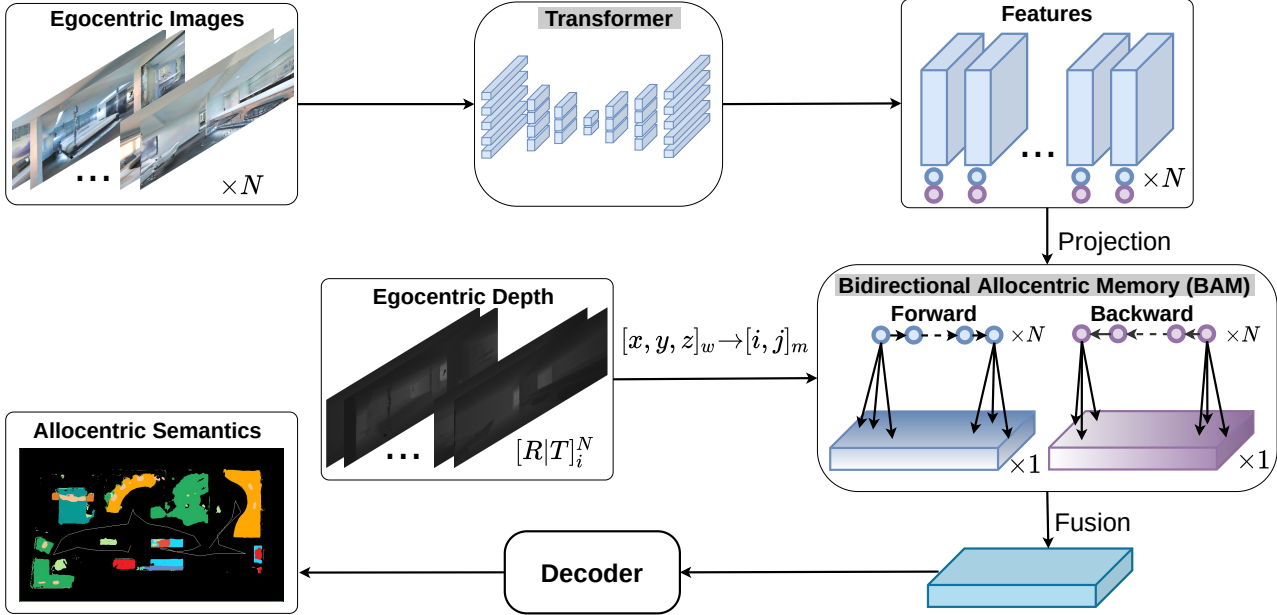


Figure 3: **The overview of the end-to-end Trans4Map framework.** There are a transformer-based encoder for extracting the egocentric features from the RGB images, a Bidirectional Allocentric Memory (BAM) to project and accumulate the extracted feature sequence to the allocentric feature map via the known depth and pose information, and a CNN-based decoder for parsing the accumulated feature and predicting the allocentric semantics.

tions. These methods do not encode depth information, so the objects on the semantic map do not reflect their geometry structure. Moreover, there are many Bird’s-Eye-view (BEV) semantic segmentation approaches for driving scene perception [3, 9, 11, 13, 21, 36, 49] emerging in the field. BEVFormer [21] aggregates spatiotemporal cues from surround-view cameras, whereas ViT-BEVSeg [10] uses a spatial transformer decoder for generating semantic occupancy grid maps. Differing from these works, we propose a transformer-based end-to-end framework, which acts as a one-stage top-down semantic mapper for holistic indoor scene understanding.

Allocentric Spatial Memory. Incrementally generating a top-view map from egocentric observations requires dynamically updating the allocentric memory, *i.e.* aggregating information over time, such as a mobile agent traveling around an indoor scene. Visual SLAM pipelines [2, 28, 40] for this task involve multiple modules such as tracking, mapping, relocalization, loop closure, and graph optimization through bundle adjustment. Recently, some learning methods have proposed a spatial memory update module which enriches the construction of maps. MapNet [15] developed a recurrent neural network which updates allocentric spatial memory per frame, and then performs registration of new observations to the previous map via dense matching. Tung *et al.* [41] proposed Geometry-aware Recurrent Neural Networks (GRNNs) to segment objects in

3D. This work is very memory-demanding due to the high-dimension features. The closest work to our approach is SMNet [4] which uses a GRU to update the projected tensor. Compared to GRNNs, their memory requirements are less stringent and better suited to understanding indoor scenes. Unlike previous works, we propose Trans4Map, a transformer-based semantic mapping framework with a bidirectional allocentric memory that can better accumulate information over time and segment occluded objects.

3. Methodology

In this section, we revisit the allocentric semantic mapping task with vision transformers and introduce our proposed end-to-end one-stage framework, that can generate allocentric semantic maps from egocentric observations.

3.1. Trans4Map: Framework Overview

As shown in Fig. 3, our end-to-end Trans4Map framework includes three steps: (1) the incoming N egocentric images are fed into the transformer-based backbone (in Sec. 3.2), which extracts contextual feature and long-range dependency; (2) the Bidirectional Allocentric Memory (BAM) module (in Sec. 3.3) projects the extracted feature via the depth-based transformation index; (3) the lightweight CNN-based decoder parses the projected feature and predicts the allocentric semantics.

The previous SMNet [4] uses a two-branch CNN-based

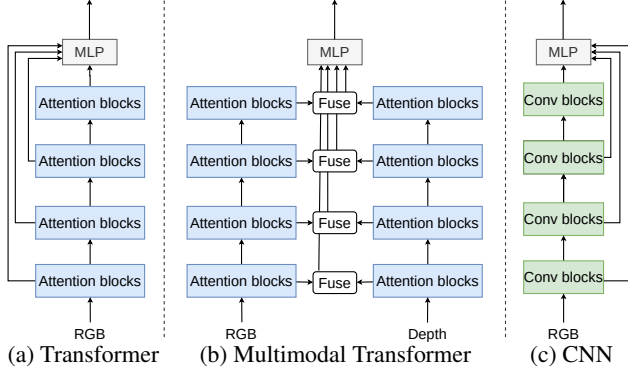


Figure 4: **Semantic mapping architectures.**

backbone to extract features from RGBD images. Due to the heavy dual-branch backbone, the data pipeline is divided into multiple stages: extracting RGBD feature maps by using a frozen encoder; storing the feature maps locally; and fine-tuning the decoder via loading the offline feature maps. Unlike such a multi-stage data flow, our framework shown in Fig. 3 operates in an end-to-end manner, benefiting from three non-trivial designs: (1) a transformer-based backbone is leveraged to capture holistic features and long-range dependencies, instead of the CNN-based backbone; (2) a single branch structure for extracting RGB features makes the whole model more lightweight than the dual-branch one; (3) an online training pipeline from egocentric images to allocentric semantics is constructed, avoiding using the time-consuming fine-tuning process and feature maps storage. Thus, our framework can achieve superior allocentric semantic mapping, while maintaining efficiency.

3.2. Transformer backbone

To fully investigate the proposed Trans4Map framework, we explore different model architectures and learning modalities for the allocentric semantic mapping task, as shown in Fig. 4. The architectures are constructed by four stages, and each stage includes a series of convolutional blocks (see Fig. 4c) or self-attention blocks (see Fig. 4a). Different from the convolutional architecture, the transformer-based architecture is able to capture non-local features, thanks to the self-attention operation [42]. Considering that cross-modality complementary features are informative for predicting semantics [16, 17, 24], we leverage RGB-Depth inputs and a multimodal architecture (see Fig. 4b) is reformed by using efficient self-attention blocks. The previous SMNet [4] has to go through a complex pipeline, because its heavy two-branch CNN backbone is overburdened by using more convolutional layers and working with memory-demanding high-resolution features twice as large as ours. They resort to a sub-optimal two-stage scheme which trains the encoder first, then freezes it to generate the offline feature map to train the decoder in the sec-

ond stage, resulting in: a complex training process; high memory requirements; inability to train synchronously. In contrast, our dual-branch model still maintains an end-to-end one-stage mapping scheme, thanks to the lightweight transformer-based backbone and the efficient framework.

For brevity, we describe the operation of the single-modal process, while the bimodal process involves an additive fusion at each stage, in which the fusion block obtains the extracted contextual features and geometry features and then fuses them per pixel with the same dimension. Given a batch of RGB images of size $N \times H \times W \times 3$, the divided patches are passed through the four-stage transformer blocks, to obtain the hierarchical feature representation with downsampling rates of $\{\frac{1}{r_1}, \frac{1}{r_2}, \frac{1}{r_3}, \frac{1}{r_4}\}$ and increasing channels of $\{C_1, C_2, C_3, C_4\}$. Then, the multi-scale features are concatenated by an MLP layer and followed by a convolution layer with 64 channels. So the hierarchical features are fused into an egocentric feature of size $N \times \frac{H}{r_1} \times \frac{W}{r_1} \times 64$. To study different semantic mapping architectures, the multi-scale features in this work are extracted with $\{\frac{1}{4}, \frac{1}{8}, \frac{1}{16}, \frac{1}{32}\}$ downsampling rates and $\{64, 128, 320, 512\}$ channels.

To compare CNN- and transformer-based models, the RedNet backbone [17] used in SMNet and the ConvNeXt backbone are selected to form CNN-based mapping models, while transformer-based models include FAN [53], Swin [25], and SegFormer [45] backbones. Based on our experiments, we adopt SegFormer [45] as the default backbone of our visual encoder, as its simple and lightweight design can generate features ranging from high-resolution fine features to low-resolution coarse features. More ablation studies and discussions are unfolded in Sec. 4.4.

3.3. Bidirectional Allocentric Memory

After acquiring the egocentric features through the aforementioned transformer backbone, the projective index is needed to project representative contextual features into an allocentric memory map. In the Habitat simulator [37], we can directly obtain the state of the moving agent and then calculate the camera pose using relative orientation and position. In order to perform the projection in Eq. (1) and Eq. (2), we need to derive the 3D position of each pixel in the egocentric image. K in Eq. (1) denotes the camera intrinsic parameter matrix, $[R|t]$ in Eq. (2) are the rotation matrix and the translation matrix, respectively. First, using the pinhole camera model and the depth of each pixel $d_{u,v}$, the pixel coordinate (u, v) in the image coordinate system can be converted into the camera coordinate system. Then, the camera coordinates denoted as (x, y, z) of each point are converted to world coordinates denoted as (X, Y, Z) using the camera pose. Each pixel in the allocentric memory map represents a $2cm \times 2cm$ cell in the scene of the Matterport3D dataset [5], so the projective index $(i, j)_m$ can be

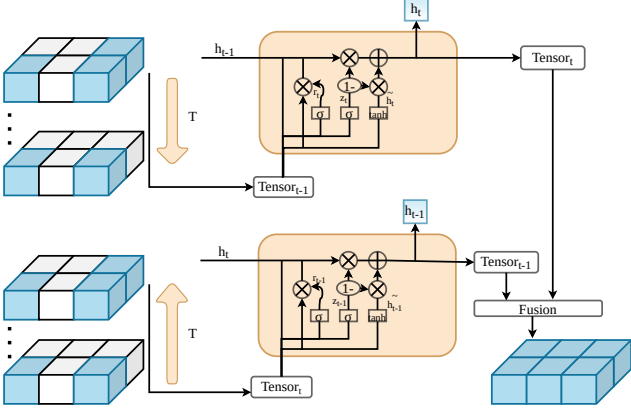


Figure 5: **Bidirectional Allocentric Memory (BAM).**

calculated by dividing the world coordinates X and Z of each point by the resolution. Finally, we project egocentric features of N batch size onto the allocentric memory map using the calculated projective index.

$$\begin{bmatrix} x \\ y \\ z \end{bmatrix}_c = K^{-1} \begin{bmatrix} u \\ v \\ d_{u,v} \end{bmatrix}_i \quad (1)$$

$$\begin{bmatrix} X \\ Y \\ Z \end{bmatrix}_w = R^{-1} \begin{bmatrix} x \\ y \\ z \end{bmatrix}_c - \vec{t} \quad (2)$$

To enhance the long-range content dependency and aggregate the incoming information completely, we propose Bidirectional Allocentric Memory (BAM), in which we transmit projected features via Bi-directional GRU (Bi-GRU), which are used to update and accumulate incoming observations from two directions. Specifically, BAM adds one more GRU unit that performs feature parsing and accumulation in reverse. As shown in Fig. 5, the upper GRU unit processes the allocentric memory tensor in a forward direction from the M^{t-1} to the M^t feature and the lower GRU unit in a backward direction from the M^t to the M^{t-1} feature. A simple yet effective convolutional layer is applied to fuse two projected allocentric memory features. The computation of updated spatial memory tensor is formulated as:

$$M_{i,j}^t = GRU(F_{i,j}^t, M_{i,j}^{t-1}); \quad (3)$$

$$M_{i,j}^{t-1} = GRU(F_{i,j}^{t-1}, M_{i,j}^t); \quad (4)$$

$$T = Conv(M_{i,j}^t, M_{i,j}^{t-1}). \quad (5)$$

$M_{i,j}^t$ and $M_{i,j}^{t-1}$ are the current time step spatial memory and previous time step spatial memory, respectively. The fused spatial memory tensors T are accessible to the decoding step for the final semantic top-down map prediction. Thanks to the bidirectional parsing process, BAM is able to accumulate the observations per each time step in both direction in parallel, thus, it can better avoid occluded objects

being wrongly-classified. With BAM, Trans4Map can produce a more meaningful allocentric representation which combines bidirectional projected features.

4. Experiment

4.1. Datasets

Matterport3D. The Matterport3D dataset [5] is a large, diverse indoor dataset that contains photo-realistic scans of 90 building-scale environments. It provides RGBD images and 3D annotations with 40 categories, which are crucial for scene understanding tasks. We follow the same dataset split as SMNet [4], consisting of 61 training scenes, 7 validation scenes, and 17 test scenes, which mainly focuses on 12 object categories: *chair, table, cushion, cabinet, shelving, sink, dresser, plant, bed, sofa, counter, fireplace*. Other rare objects and floor surfaces are masked as void classes. Given a trajectory, we sample 50 sets of N consecutive waypoints in each unique scene, with which we can obtain the agent state and RGBD rendering with the Habitat simulator [37]. Then, the N consecutive RGBD image sequences as a batch are forwarded into the model as input.

Replica. The Replica dataset [39] contains 18 various highly photo-realistic indoor environments. It provides dense-mesh, high-resolution RGBD images and also a large range of instance annotations with 88 categories. We follow the same setup as in the Matterport3D dataset, *i.e.*, focusing on 12 object categories. We test our model on the Replica using the weight that was trained on Matterport3D dataset, so the 18 scenes are included in the test split.

4.2. Implementation details

Performing the encode-project-segment paradigm, we train our model in an end-to-end manner. For the ablation study, we revisit the transformer-based mapping and investigate several visual encoders in our model which are pretrained on the ImageNet [35] and ADE20K [52], and the BAM module and the decoder are randomly initialized. We use the AdamW optimizer [19] to train our model with four 1080Ti GPUs on the Matterport3D dataset. The learning rate is initialized with $6e^{-5}$ and then scheduled by LambdaLR. Training with 100 epochs will take about 30 hours. Similar to [4], the evaluation metrics include the pixel-wise accuracy (Acc), the pixel recall (mRecall) and precision (mPrecision) scores, the intersection-over-union (mIoU) score, and the boundary F1 (mBF1) score [8].

4.3. Allocentric semantic mapping results

As shown in Table 1 and Table 2, a set of results are compared in different mapping paradigms. In the project-segment paradigm, the egocentric images are converted into top-down images using homography-based projection [1] and then perform semantic segmentation. This method

Table 1: **Allocentric semantic mapping results** on the Matterport3D dataset. Model[†] is our implementation.

Method	Acc	mRecall	mPrecision	mIoU	mBF1
Seg. GT → Proj.	89.49	73.73	74.58	59.73	54.05
Proj. → Seg.	83.18	27.32	35.30	19.96	17.33
Seg. → Proj.	88.06	40.53	58.92	32.76	33.21
Semantic SLAM	85.17	37.51	51.54	28.11	31.05
SMNet	88.14	47.49	58.27	36.77	37.02
SMNet [†]	89.14	46.34	56.98	36.16	35.95
Trans4Map	89.02	54.50	56.20	40.02	41.11

Table 2: **Allocentric semantic mapping results** on the Replica dataset. Model[†] is our implementation.

Method	Acc	mRecall	mPrecision	mIoU	mBF1
Seg. GT → Proj.	96.83	83.84	94.05	79.76	86.89
Seg. → Proj.	88.61	48.11	65.20	40.77	45.86
Semantic SLAM	88.30	45.80	62.41	37.99	46.71
SMNet	89.26	53.37	64.81	43.12	45.18
SMNet [†]	87.69	58.88	34.85	27.68	42.67
Trans4Map	86.19	65.27	34.91	29.15	48.66

performs relatively poorly in terms of mIoU and mBF1, whereas the segment-project paradigm starts with semantic segmentation of egocentric images and then projects labels or extracted features into a top-down mapping. Our Trans4Map follows the aforementioned encode-project-segment paradigm [4].

Matterport3D. The results of top-down semantic segmentation on the Matterport3D dataset are presented in Table 1. Following the segment-project paradigm, the result obtained by using the label data is the upper bound performance. As in Table 1, the segment-project baseline performs much better than the project-segment one, since part of information will be lost in the process of converting an egocentric image into a top-down view. The semantic SLAM in [14] also uses the segment-project method but achieves worse performance than the image-based segment-project baseline. SMNet [4] follows the encode-project-segment paradigm and adds a spatial memory update module. Here, we reproduce the experiment using the released code under the same condition and obtain the results with a mIoU score of 36.16% and a mBF1 value of 35.95%. Compared to SMNet, our Trans4Map model achieves significant improvements in terms of mIoU (40.02%) and mBF1 (41.11%) on the Matterport3D dataset, which proves the effectiveness of our proposed allocentric mapping framework.

Replica. To further compare the performance of different semantic mapping methods, the top-down semantic segmentation results on the Replica dataset are reported in Table 2. All models are trained on the Matterport3D dataset and tested on the Replica dataset. Note that the trajectories and labels of the Replica dataset are partially available at the

Table 3: **Comparison of different backbones** including the number of parameters and performance on Matterport3D.

Method	Backbone	#Param (M)	mIoU (%)
SMNet	RedNet [4]	83.9	36.77
ConvNeXt	ConvNeXt-T [26]	31.1	35.91
ConvNeXt	ConvNeXt-S [26]	52.7	36.49
FAN	FAN-T [53]	09.8	31.07
FAN	FAN-S [53]	31.3	34.62
Swin	Swin-T [25]	30.8	34.19
Swin	Swin-S [25]	52.1	36.80
Trans4Map	MiT-B1 [45]	15.4	34.38
Trans4Map	MiT-B2 [45]	27.5 (-56.4)	40.02 (+3.25)
Trans4Map	MiT-B3 [45]	47.4 (-36.5)	39.98 (+3.21)
Trans4Map	MiT-B4 [45]	64.1 (-19.8)	40.88 (+4.11)

moment, thus, the results are tested on the constrained data of the Replica dataset. Nonetheless, under the same condition with the same label data, our Trans4Map outperforms the baseline SMNet with a 1.47% mIoU and a 5.99% mBF1 improvements, respectively. The results indicate that our Trans4Map framework achieves consistent improvements across different datasets.

4.4. Ablation study

Analysis of Encoder. We first analyze the effects of using different backbones to extract features. We investigate a vast number of backbones which are either CNN-based or transformer-based. All the encoders forward the same input and extract contextual features with the same dimensions. The input for all encoders is a batch of four consecutive images observed from four consecutive waypoints along a trajectory during training. As shown in Table 3, SMNet using CNN-based RedNet as backbone, which is pretrained on SUN-RGBD, has the most parameters compared to other backbones. Due to the overburdened backbone, the SMNet relies on a multi-stage process, resulting the mapping inefficient. It achieves 36.77% in mIoU. We test two other versions of CNN-based backbones, *i.e.*, ConvNeXt-T and ConvNeXt-S, which are pretrained on ImageNet. Compared to SMNet, ConvNeXt-T has only 37.1% of the parameters but can achieve comparable results. For transformer-based comparison counterparts, we mainly investigate FAN [53], Swin [25], and SegFormer [45] backbones. The parameters of FAN-S and Swin-T are similar, and the obtained results are comparable. Our Trans4Map equipped with the MiT-B2 backbone [45] reduces 67.2% parameters compared to SMNet, *i.e.*, from 83.9M to 27.5M, but the performance has made a sufficient leap in mIoU (+3.25%). The MiT-B3 and -B4 backbone with 47.4M and 64.1M parameters bring similar mIoU gains (+3.21% and +4.11%) as the MiT-B2 backbone, because a larger transformer model often requires more training data to obtain a desired boost. Based on the experi-



Figure 6: **Allocentric semantic mapping visualizations.** There are two indoor scenes from the Matterport3D test set. From left to right are the predicted results of SMNet, the results of our Trans4Map and the ground truth. Zoom in for better view.

Table 4: Ablation study of the BAM in Trans4Map. Models are trained with four sampling points in a trajectory.

Method	mIoU
① BiGRU + Concatenate	36.73
② BiGRU + 2 GRUCells + Conv Fusion	40.00
③ BiGRU + gMLP [22] + Conv Fusion	40.15
④ BiGRU + Conv Fusion (our BAM)	40.44

ments, the Trans4Map with MiT-B2 maintains the desired performance in the trade-off of the accuracy and efficiency.

Analysis of BAM. Apart from the encoder, we further analyze the influence of different BiGRU-based structures for our *BAM* module. As shown in Table 4, the method (①) concatenates the bidirectional spatial tensors and achieves 36.73% mIoU. The method (②) equipped with two GRU unit cells obtains 40.00% in mIoU. The method (③) is to follow an advanced gMLP block [22] for token information mixing after the BiGRU module and yields a mIoU of 40.15%. Our *BAM* (④) applies a simple yet effective convolutional layer to fuse the two updated spatial tensors. This structure is more lightweight compared to the previous ones

and achieves the best performance with 40.44% in mIoU.

Analysis of pre-train sources. The source dataset used for pre-training plays an important role in obtaining initialization weights. Here, we ablate three different pre-train sources. As shown in Table 5, comparing ② and ③, Trans4Map model benefits more from the SUN-RGBD dataset than from the ADE20K dataset, since the pre-trained weights from ADE20K are shared between the RGB and depth branches, while the ones from SUN-RGBD are separated. Between ① and ④, both Trans4Map models pre-trained on ImageNet and ADE20K have comparable results. It indicates that our single-modal Trans4Map is stable and robust across different pre-training settings.

Analysis of sampling points. The number of sampling points is a key factor in obtaining dense observations. Theoretically, as the sequence of input images increases, the richer the resulting map will be. In ④ and ⑤ of Table 5, increasing the number of sampling points from 4 to 20, Trans4Map with MiT-B2 benefits from the dense observations and obtains a gain of +2.31% in mIoU. Comparing ⑧ and ⑨, the consistent improvement is achieved by Trans4Map with MiT-B4.

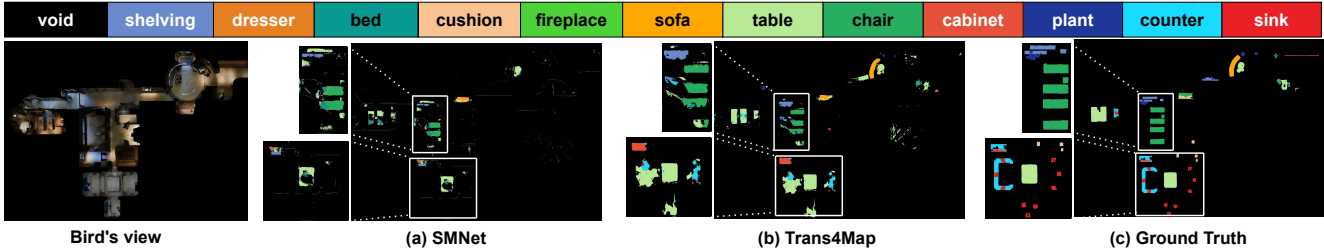


Figure 7: Visualizations of the challenging case. Zoom in for better view.

Table 5: Analysis of model complexities, data sources, sampling points in a trajectory, and data modalities.

	Method	Pre-train	#Points	Modality	mIoU
	SMNet [4]	SUN-RGBD	20	RGBD	36.77
1	B2	ImageNet	4	RGB	37.86
2	B2	SUN-RGBD	4	RGBD	40.27
3	B2	ADE20K	4	RGBD	40.15
4	B2	ADE20K	4	RGB	37.71
5	B2	ADE20K	20	RGB	40.02
6	B3	ADE20K	4	RGB	38.78
7	B3	ADE20K	20	RGB	39.98
8	B4	ADE20K	4	RGB	40.44
9	B4	ADE20K	20	RGB	40.88

Analysis of data modalities. To ablate the effect of data modalities, RGB and RGBD inputs are compared by using single-modal and dual-modal Trans4Map. Compared between the RGBD baseline SMNet and 2 in Table 5, our dual-modal Trans4Map has a 3.5% mIoU gain, while both are trained on SUN-RGBD. When using 4 sampling points, the dual-modal Trans4Map performs better than the single-modal one, as compared in 3 and 4. It indicates the effectiveness of our dual-modal Trans4Map in harvesting cross-stream complementary features for boosting performance.

Analysis of model complexities. To inspect the trade-off between efficiency and performance, we analyze the model complexity by using three different backbones, *i.e.*, MiT-B2, -B3 and -B4. They have respective 27.5M, 47.4M and 64.1M parameters, yet all are more lightweight than the baseline SMNet with 83.9M, as presented in Table. 3. Comparing three backbones (4, 6, 8), larger models have better results, since more training data is available based on 4 sampling points. In the case of 20 sampling points (5, 7, 9), the three models achieve competitive results compared to the baseline model. This experiment demonstrates the effectiveness of our Trans4Map framework, achieving consistent improvements based on backbones of different sizes.

4.5. Qualitative analysis

Semantic map visualizations. To compare our Trans4Map with the baseline SMNet, we visualize the allocentric semantic map results, as shown in Fig. 6. All the compared scenes are selected from the test set of the Matter-

port3D dataset. Thanks to the extracted non-local features and long-distance dependencies, Trans4Map has much better segmentation results on the overall top-down semantic maps. In the first scene shown in Fig. 6, Trans4Map is better at segmenting the *bed* with a more complete and accurate mask, as compared to SMNet. Further, Trans4Map is able to successfully classify the *fireplace*, while the baseline model fails and predicts it as a *cabinet*. In the second scene in Fig. 6, we notice that Trans4Map performs allocentric semantic mapping accurately, such as on *cabinet* and *chair* categories, while SMNet misclassifies them as *tables*. Besides, SMNet yields incomplete *chair* segmentation results. **Challenging case analysis.** The allocentric semantic mapping in the large-scale indoor scenes is still a challenging task. Fig. 7 demonstrates that both models struggle with semantic mapping in such a large-scale scene. In particular, SMNet has difficulty segmenting the four *chairs* completely as shown in the zoom-in region in Fig. 7 (a). Our Trans4Map performs slightly better, but there is still a large improvement space. In the lower part of the top-down map, both models perform poorly. All the six *sinks* (in red colors) are not predicted correctly. The reason is that the depth information of this scene is less reliable to support the projection process, while the whole scene covers about 2500 square meters on the allocentric map. One potential solution is to obtain more observations to alleviate the error caused by the noisy depth measurements.

5. Conclusion

In this paper, we propose an end-to-end transformer-based framework, termed *Trans4Map*, in order to revisit the egocentric-to-allocentric mapping from the front-view images to top-view semantics. Based on the transformer-driven backbone and the *Bidirectional Allocentric Memory (BAM)* updater, Tran4Map sets the new state of the art on both Matterport3D and Replica datasets, while using a more lightweight architecture and having fewer parameters as compared to the previous work. In the future, we will further explore domain adaptation methods to transfer the mapping models trained on the synthetic datasets to real-world scenes. Based on the constructed semantic map, the downstream tasks such as indoor navigation and path planning will also be interesting research directions.

References

- [1] Syed Ammar Abbas and Andrew Zisserman. A geometric approach to obtain a bird’s eye view from an image. In *ICCVW*, 2019. 5
- [2] Carlos Campos, Richard Elvira, Juan J. Gómez Rodríguez, José M. M. Montiel, and Juan D. Tardós. ORB-SLAM3: An accurate open-source library for visual, visual–inertial, and multimap SLAM. *T-RO*, 2021. 3
- [3] Yigit Baran Can, Alexander Liniger, Danda Pani Paudel, and Luc Van Gool. Structured bird’s-eye-view traffic scene understanding from onboard images. In *CVPR*, 2021. 3
- [4] Vincent Cartillier, Zhile Ren, Neha Jain, Stefan Lee, Irfan Essa, and Dhruv Batra. Semantic MapNet: Building allocentric semantic maps and representations from egocentric views. In *AAAI*, 2021. 1, 2, 3, 4, 5, 6, 8
- [5] Angel Chang, Angela Dai, Thomas Funkhouser, Maciej Halber, Matthias Niessner, Manolis Savva, Shuran Song, Andy Zeng, and Yinda Zhang. Matterport3D: Learning from RGB-D data in indoor environments. In *3DV*, 2017. 2, 4, 5
- [6] Devendra Singh Chaplot, Dhiraj Gandhi, Saurabh Gupta, Abhinav Gupta, and Ruslan Salakhutdinov. Learning to explore using active neural SLAM. In *ICLR*, 2020. 1
- [7] Hao Chen, Weijian Hu, Kailun Yang, Jian Bai, and Kaiwei Wang. Panoramic annular SLAM with loop closure and global optimization. *AO*, 2021. 1
- [8] Gabriela Csurka, Diane Larlus, Florent Perronnin, and France Meylan. What is a good evaluation measure for semantic segmentation?. In *BMVC*, 2013. 5
- [9] Alexey Dosovitskiy, Lucas Beyer, Alexander Kolesnikov, Dirk Weissenborn, Xiaohua Zhai, Thomas Unterthiner, Mostafa Dehghani, Matthias Minderer, Georg Heigold, Sylvain Gelly, Jakob Uszkoreit, and Neil Houlsby. An image is worth 16x16 words: Transformers for image recognition at scale. In *ICLR*, 2021. 2, 3
- [10] Pramit Dutta, Ganesh Sistu, Senthil Yogamani, Edgar Galván, and John McDonald. ViT-BEVSeg: A hierarchical transformer network for monocular birds-eye-view segmentation. In *IJCNN*, 2022. 3
- [11] Isht Dwivedi, Srikanth Malla, Yi-Ting Chen, and Behzad Dariush. Bird’s eye view segmentation using lifted 2D semantic features. In *BMVC*, 2021. 3
- [12] Georgios Georgakis, Bernadette Bucher, Karl Schmeckpeper, Siddharth Singh, and Kostas Daniilidis. Learning to map for active semantic goal navigation. In *ICLR*, 2022. 1
- [13] Nikhil Gosala and Abhinav Valada. Bird’s-eye-view panoptic segmentation using monocular frontal view images. *RA-L*, 2022. 3
- [14] Margarita Grinvald, Fadri Furrer, Tonci Novkovic, Jen Jen Chung, Cesar Cadena, Roland Siegwart, and Juan Nieto. Volumetric instance-aware semantic mapping and 3D object discovery. *RA-L*, 2019. 1, 2, 6
- [15] João F. Henriques and Andrea Vedaldi. MapNet: An allocentric spatial memory for mapping environments. In *CVPR*, 2018. 3
- [16] Xinxin Hu, Kailun Yang, Lei Fei, and Kaiwei Wang. ACNet: Attention based network to exploit complementary features for RGBD semantic segmentation. In *ICIP*, 2019. 4
- [17] Jindong Jiang, Lunan Zheng, Fei Luo, and Zhijun Zhang. RedNet: Residual encoder-decoder network for indoor rgb-d semantic segmentation. *arXiv preprint arXiv:1806.01054*, 2018. 4
- [18] Kapil D. Katyal, Adam Polevoy, Joseph L. Moore, Craig Knuth, and Katie M. Popek. High-speed robot navigation using predicted occupancy maps. In *ICRA*, 2021. 1
- [19] Diederik P. Kingma and Jimmy Ba. Adam: A method for stochastic optimization. In *ICLR*, 2015. 5
- [20] Diederik P. Kingma and Max Welling. Auto-encoding variational bayes. In *ICLR*, 2014. 2
- [21] Zhiqi Li, Wenhai Wang, Hongyang Li, Enze Xie, Chonghao Sima, Tong Lu, Qiao Yu, and Jifeng Dai. BEVFormer: Learning bird’s-eye-view representation from multi-camera images via spatiotemporal transformers. In *ECCV*, 2022. 3
- [22] Hanxiao Liu, Zihang Dai, David R. So, and Quoc V. Le. Pay attention to MLPs. In *NeurIPS*, 2021. 7
- [23] Huayao Liu, Ruiping Liu, Kailun Yang, Jiaming Zhang, Kunyu Peng, and Rainer Stiefelwagen. HIDA: Towards holistic indoor understanding for the visually impaired via semantic instance segmentation with a wearable solid-state lidar sensor. In *ICCVW*, 2021. 1
- [24] Huayao Liu, Jiaming Zhang, Kailun Yang, Xinxin Hu, and Rainer Stiefelwagen. CMX: Cross-modal fusion for RGB-X semantic segmentation with transformers. *arXiv preprint arXiv:2203.04838*, 2022. 4
- [25] Ze Liu, Yutong Lin, Yue Cao, Han Hu, Yixuan Wei, Zheng Zhang, Stephen Lin, and Baining Guo. Swin transformer: Hierarchical vision transformer using shifted windows. In *ICCV*, 2021. 2, 4, 6
- [26] Zhuang Liu, Hanzhi Mao, Chao-Yuan Wu, Christoph Feichtenhofer, Trevor Darrell, and Saining Xie. A ConvNet for the 2020s. In *CVPR*, 2022. 2, 6
- [27] Chenyang Lu, Marinus Jacobus Gerardus van de Molengraft, and Gijs Dubbelman. Monocular semantic occupancy grid mapping with convolutional variational encoder-decoder networks. *RA-L*, 2019. 2
- [28] Raul Mur-Artal, Jose Maria Martinez Montiel, and Juan D Tardos. ORB-SLAM: A versatile and accurate monocular SLAM system. *T-RO*, 2015. 3
- [29] Wenyan Ou, Jiaming Zhang, Kunyu Peng, Kailun Yang, Gerhard Jaworek, Karin Müller, and Rainer Stiefelwagen. Indoor navigation assistance for visually impaired people via dynamic SLAM and panoptic segmentation with an RGB-D sensor. In *ICCHP-AAATE*, 2022. 1
- [30] Bowen Pan, Jiankai Sun, Ho Yin Tiga Leung, Alex Andonian, and Bolei Zhou. Cross-view semantic segmentation for sensing surroundings. *RA-L*, 2020. 2
- [31] Kunyu Peng, Juncong Fei, Kailun Yang, Alina Roitberg, Jiaming Zhang, Frank Bieder, Philipp Heidenreich, Christoph Stiller, and Rainer Stiefelwagen. MASS: Multi-attentional semantic segmentation of LiDAR data for dense top-view understanding. *T-ITS*, 2022. 1
- [32] Kunyu Peng, Alina Roitberg, Kailun Yang, Jiaming Zhang, and Rainer Stiefelwagen. TransDARC: Transformer-based driver activity recognition with latent space feature calibration. In *IROS*, 2022. 2

- [33] Santhosh K Ramakrishnan, Ziad Al-Halah, and Kristen Grauman. Occupancy anticipation for efficient exploration and navigation. In *ECCV*, 2020. 1
- [34] Teng Ran, Liang Yuan, Jianbo Zhang, Dingxin Tang, and Li He. RS-SLAM: A robust semantic SLAM in dynamic environments based on RGB-D sensor. *IEEE Sensors Journal*, 2021. 2
- [35] Olga Russakovsky, Jia Deng, Hao Su, Jonathan Krause, Sanjeev Satheesh, Sean Ma, Zhiheng Huang, Andrej Karpathy, Aditya Khosla, Michael S. Bernstein, Alexander C. Berg, and Li Fei-Fei. ImageNet large scale visual recognition challenge. *IJCV*, 2015. 5
- [36] Avishkar Saha, Oscar Mendez Maldonado, Chris Russell, and Richard Bowden. Translating images into maps. In *ICRA*, 2022. 3
- [37] Manolis Savva, Jitendra Malik, Devi Parikh, Dhruv Batra, Abhishek Kadian, Oleksandr Maksymets, Yili Zhao, Erik Wijmans, Bhavana Jain, Julian Straub, Jia Liu, and Vladlen Koltun. Habitat: A platform for embodied AI research. In *ICCV*, 2019. 2, 4, 5
- [38] Suriya Singh, Anil Batra, Guan Pang, Lorenzo Torresani, Saikat Basu, Manohar Paluri, and C. V. Jawahar. Self-supervised feature learning for semantic segmentation of overhead imagery. In *BMVC*, 2018. 2
- [39] Julian Straub, Thomas Whelan, Lingni Ma, Yufan Chen, Erik Wijmans, Simon Green, Jakob J. Engel, Raul Mur-Artal, Carl Ren, Shobhit Verma, Anton Clarkson, Mingfei Yan, Brian Budge, Yajie Yan, Xiaqing Pan, June Yon, Yuyang Zou, Kimberly Leon, Nigel Carter, Jesus Briales, Tyler Gillingham, Elias Mueggler, Luis Pesqueira, Manolis Savva, Dhruv Batra, Hauke M. Strasdat, Renzo De Nardi, Michael Goesele, Steven Lovegrove, and Richard A. Newcombe. The replica dataset: A digital replica of indoor spaces. *arXiv preprint arXiv:1906.05797*, 2019. 2, 5
- [40] Sebastian Thrun. Probabilistic robotics. *Communications of the ACM*, 2002. 3
- [41] Hsiao-Yu Fish Tung, Ricson Cheng, and Katerina Fragkiadaki. Learning spatial common sense with geometry-aware recurrent networks. In *CVPR*, 2019. 3
- [42] Ashish Vaswani, Noam Shazeer, Niki Parmar, Jakob Uszkoreit, Llion Jones, Aidan N. Gomez, Łukasz Kaiser, and Illia Polosukhin. Attention is all you need. In *NeurIPS*, 2017. 2, 4
- [43] Qing Wang, Jiaming Zhang, Kailun Yang, Kunyu Peng, and Rainer Stiefelhagen. MatchFormer: Interleaving attention in transformers for feature matching. *arXiv preprint arXiv:2203.09645*, 2022. 2
- [44] Wenhai Wang, Enze Xie, Xiang Li, Deng-Ping Fan, Kaitao Song, Ding Liang, Tong Lu, Ping Luo, and Ling Shao. Pyramid vision transformer: A versatile backbone for dense prediction without convolutions. In *ICCV*, 2021. 2
- [45] Enze Xie, Wenhai Wang, Zhiding Yu, Anima Anandkumar, Jose M. Alvarez, and Ping Luo. SegFormer: Simple and efficient design for semantic segmentation with transformers. In *NeurIPS*, 2021. 2, 4, 6
- [46] Weixiang Yang, Qi Li, Wenxi Liu, Yuanlong Yu, Yuexin Ma, Shengfeng He, and Jia Pan. Projecting your view at- tentively: Monocular road scene layout estimation via cross-view transformation. In *CVPR*, 2021. 1
- [47] Jiaming Zhang, Kailun Yang, Angela Constantinescu, Kunyu Peng, Karin Müller, and Rainer Stiefelhagen. Trans4Trans: Efficient transformer for transparent object and semantic scene segmentation in real-world navigation assistance. *TITS*, 2022. 2
- [48] Jiaming Zhang, Kailun Yang, Chaoxiang Ma, Simon Reiß, Kunyu Peng, and Rainer Stiefelhagen. Bending reality: Distortion-aware transformers for adapting to panoramic semantic segmentation. In *CVPR*, 2022. 1
- [49] Yun Zhao, Yu Zhang, Zhan Gong, and Hong Zhu. Scene representation in bird’s-eye view from surrounding cameras with transformers. In *CVPR*, 2022. 3
- [50] Sixiao Zheng, Jiachen Lu, Hengshuang Zhao, Xiatian Zhu, Zekun Luo, Yabiao Wang, Yanwei Fu, Jianfeng Feng, Tao Xiang, Philip H. S. Torr, and Li Zhang. Rethinking semantic segmentation from a sequence-to-sequence perspective with transformers. In *CVPR*, 2021. 2
- [51] Brady Zhou and Philipp Krähenbühl. Cross-view transformers for real-time map-view semantic segmentation. In *CVPR*, 2022. 1
- [52] Bolei Zhou, Hang Zhao, Xavier Puig, Sanja Fidler, Adela Barriuso, and Antonio Torralba. Scene parsing through ADE20K dataset. In *CVPR*, 2017. 5
- [53] Daquan Zhou, Zhiding Yu, Enze Xie, Chaowei Xiao, Anima Anandkumar, Jiashi Feng, and Jose M. Alvarez. Understanding the robustness in vision transformers. In *ICML*, 2022. 2, 4, 6